IRANIAN JOURNAL OF PHYSICS RESEARCH

Iranian Journal of Physics Research, Vol. 8, No. 4, 2009

Energy dependent fractal dimension in lateral electron distribution of extensive air showers

D Purmohammad and F Bahreini Davarani

Faculty of Science, Imam Khomeini International University, PO Box 34149-16818 , Qazvin, Iran

(Received 16 August 2008 ; In final form 17 January 2009)

Abstract

Secondary electrons at ground level of simulated extensive air showers have been analyzed using a wavelet transform based technique, in order to investigate the variation of fractal dimensions of the lateral distribution of the electrons with shower energy and primary particle mass number. The fractal dimension is shown to increase with shower energy and seems to saturate to constant values near the core of the shower at higher energies. Using the fractal dimension properties at different core distances, a multi-parameter separation technique is then applied to the data. It has been shown that the technique has good accuracy at high energy, provided the energy of the shower is obtained independently.

Keywords: cosmic rays, extensive air showers

1. Introduction

High energy radiation, including gamma rays and cosmic rays (CR) have a steep energy spectrum. At energies above 10^{12}eV, the flux of the radiation is too low to be observable by space borne small detectors. High probability of interaction with air nuclei prevents these high energy particles reaching ground based detectors. The interactions develop avalanches of secondary particles, such as electrons, photons, muons, nucleons and other hadrons which form an extensive air shower (EAS). Particle detector arrays, covering areas from 100 to a few thousand km^2, are being used to detect the secondary particles in the shower [1, 2]. Other detection techniques utilize low energy radiation from the secondary particles. Cherenkov radiation [3], air fluorescence [4], and radio emission [5] generated by shower particles can be detected in order to infer the EAS properties. The main goal of such observations is estimation of the primary particle type, energy, and direction. Since the development of EAS results from a huge number of interactions, the observable shower parameters which are sensitive to the place and type of interactions, behave stochastically. Monte Carlo simulations are widely used in EAS studies. Despite considerable theoretical studies on the origin of high energy CR [6]-[9], the mass spectrum of the observed CR has to be studied more carefully in order to confirm the high energy cosmic ray acceleration candidates [10, 11]. Background CR elimination is important in ground-based gamma ray astronomy. Differences in the muon content of EAS are often used to discriminate the primary particles [12]-[15]. Lateral distribution of shower components (electromagnetic, muonic, hadronic)[16]-[18], as well as longitudinal profile of showers [19] has been utilized for shower type discrimination. Among these are separation techniques based on fractal dimension of electron distribution in the shower core region [20]-[25]. A wavelet transform-based fractal dimension has been shown to be suitable for shower type discrimination at 10^{14}eV [20]. The present work addresses the question about the dependence of the fractal dimension on the shower energy, by computing the fractal dimension of the electron distribution for 1200 simulated EAS at 10^{14}eV, and 10^{16}eV energies. In order to extend the separation technique based on the fractal dimension, energy dependent parameters have been introduced.

2. Fractal analysis on simulated showers

2.1. Fractal dimension revealed by wavelet transform

It has been shown [26, 27] that fractal dimension of a function can be revealed by its wavelet transformation. Rastegarzadeh and Samimi [20] have used the idea to investigate the local fractal dimension of the electron density function. Here we use their technique as follows. If the density function, $f(x,y)$, has any fractal property, its two-dimensional wavelet transform in an annular region, $r_i < r \le r_o$ centered at the shower core, defined by

$$T(a,b_x,b_y) = \iint_{x^2+y^2>r_i^2}^{x^2+y^2\le r_o^2} g(x,y;a,b_x,b_y)\, f(x,y)\, dx\, dy \quad , \tag{1}$$

will behave like

$$T(a,b_x,b_y) \sim a^{\alpha(b_x,b_y)} , \tag{2}$$

in which α is the fractal dimension in that region. In the eq. (1), a two dimensional Mexican hat wavelet:

$$g(x,y;a;b_x,b_y) = [1-\frac{(x-b_x)^2}{2a^2}-\frac{(y-b_y)^2}{2a^2}]\exp[-\frac{(x-b_x)^2}{2a^2}-\frac{(y-b_y)^2}{2a^2}], \tag{3}$$

with a as scaling, b_x and b_y as translational parameters, has been used. Since the simulation code can provide the location of each secondary electron, the density function at any point has been calculated numerically.

2.2. Results of fractal analysis on simulated showers

In this work, CORSIKA shower simulation code [28] has been used with QGSJET hadronic interaction model. In order to study the dependence of the fractal dimension on both the energy and the mass number of the progenitors of the extensive air showers, 1200 showers has been simulated consisting of 100 showers for each fix primary type and energy, including gamma-ray, proton, aluminum, and iron initiated showers with 10^{14}eV, 10^{15}eV, and 10^{16}eV energies. All primary particles in the simulation had zero zenith angle. The two dimensional wavelet transformation was then applied to the secondary $e^{\pm}$ density function of each shower at observation level (1200 m in Tehran). For 100 random positions (b_x,b_y) in each annular region, $T(a;b_x,b_y)$ was numerically computed. For all the wavelet transforms results, We have obtained $T(a;b_x,b_y) \propto a^{\alpha}$ with a core distance dependent exponent α. Thus the linear $\ln T - \ln a$ property reported by [20] for 10^{14}eV showers, was confirmed to be valid in 10^{15}eV and 10^{16}eV showers too. In addition to the core distance dependence of the fractal dimension, reported before in 10^{14}eV showers [20], the present work reveals the dependence of the fractal dimension on the energy of the shower for the fix primary type and core distance. In all showers in the present work the obtained α values have normal distribution. The mean and standard deviation of such distributions are useful parameters that can be used for shower type discrimination (see section 3). For all showers of the same type and energy, the average fractal dimension in each region, has been computed. The results are presented in figures 1 to 5. The standard deviation $(\overline{\sigma})$ of these distributions is also presented as vertical error bars of the data points.

The dependence of these average fractal dimensions on the primary particle mass number, for different energies, in the regions within 10 meter from the shower core is presented in figure 1. Variation of α versus shower energy, for different primary types in the same region is shown in the figure 2. It can be seen in the figure 1 that α increases with energy at all core distances. The difference between average fractal dimensions $(\overline{\mu})$ in the same region for different mass numbers decrease with energy. The error bars $(\overline{\sigma})$ too, decreases with energy.

At higher primary energies the core regions have very high $e^{\pm}$ surface densities, and the fractal dimensions seem to be saturated. Since the lateral size of the 10^{16}eV showers are considerably higher than 10^{14}eV showers, we have tried the fractal analysis on farther regions from the core of the showers, in annuli with $20\text{m} < \text{r} \le 30\text{m}$, $50\text{m} < \text{r} \le 60\text{m}$, and $100\text{m} < \text{r} \le 110\text{m}$. The computed fractal dimensions at these annuli are presented in the figure 3 and figure 4.

For 10^{14}eV showers there are few electrons at far core distances, and thus the fractal dimension vanishes. At this far regions the difference between gamma-ray and cosmic-ray induced showers are considerable even at highest energy compared to the differences near the core. In the 5 variation of α with the distance from the shower core for three energies are presented. It clearly shows that in the highest energy, the fractal dimension near the core converges to the same value for all shower types.

3. Application of the multivarable separation technique

Since the α values overlap for different shower types, we can not use them as a single parameter discriminator. The average and standard deviation of fractal dimension at two regions of each shower have been used to improve the discrimination confidence. In each region and for each of the simulated showers, the mean, μ, and standard deviation, σ, for the normal distribution of the fractal dimension, have been computed. These parameters at two different regions, $0 < \text{r} \le 3\text{m}$ and $8\text{m} < \text{r} \le 10\text{m}$ have been used in [20] to establish a multi-variable separation technique. In order to check the validity of the method for higher energy showers, we applied the same 4-variable mass estimation function:

$$M_{est} = p_1(\mu_I\mu_O - \sigma_I\sigma_O)^{-1} + p_2(\mu_I^2 - \sigma_I^2)^{-1}(\mu_o^2 - \sigma_O^2)^{-1} \quad , \tag{4}$$

M_{est} is the estimated mass number of the primary particle, μ_I is the mean, and σ_I is the standard deviation of the computed α values in the region $0 < \text{r} \le 3\text{m}$ around the shower core. μ_O and σ_O are the same quantities obtained for $8\text{m} < \text{r} \le 10\text{m}$. It has been found that no single pairs of p_1 and p_2 can give a suitable estimation function applicable to all primary

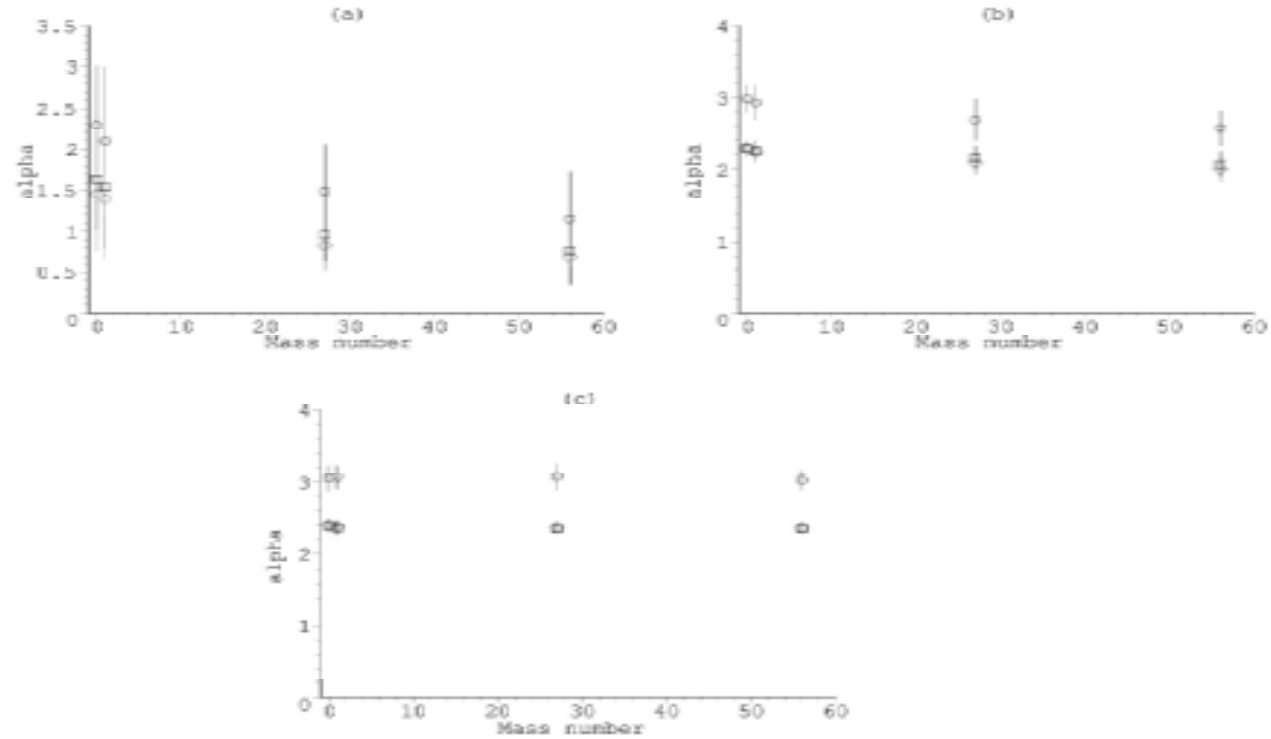

Figure 1. Computed fractal dimension (α) vs. mass number of primary particle for three energies: (a) for 10^{14}eV, (b) for 10^{15}eV, and (c) for 10^{16}eV showers. Circles, Boxes, and diamonds represent the data in annuli defined by $0 \le r \le 3m$, $4m < r \le 6m$, and $8m < r \le 10m$ respectively. Vertical error bars are standard deviation of the data points.

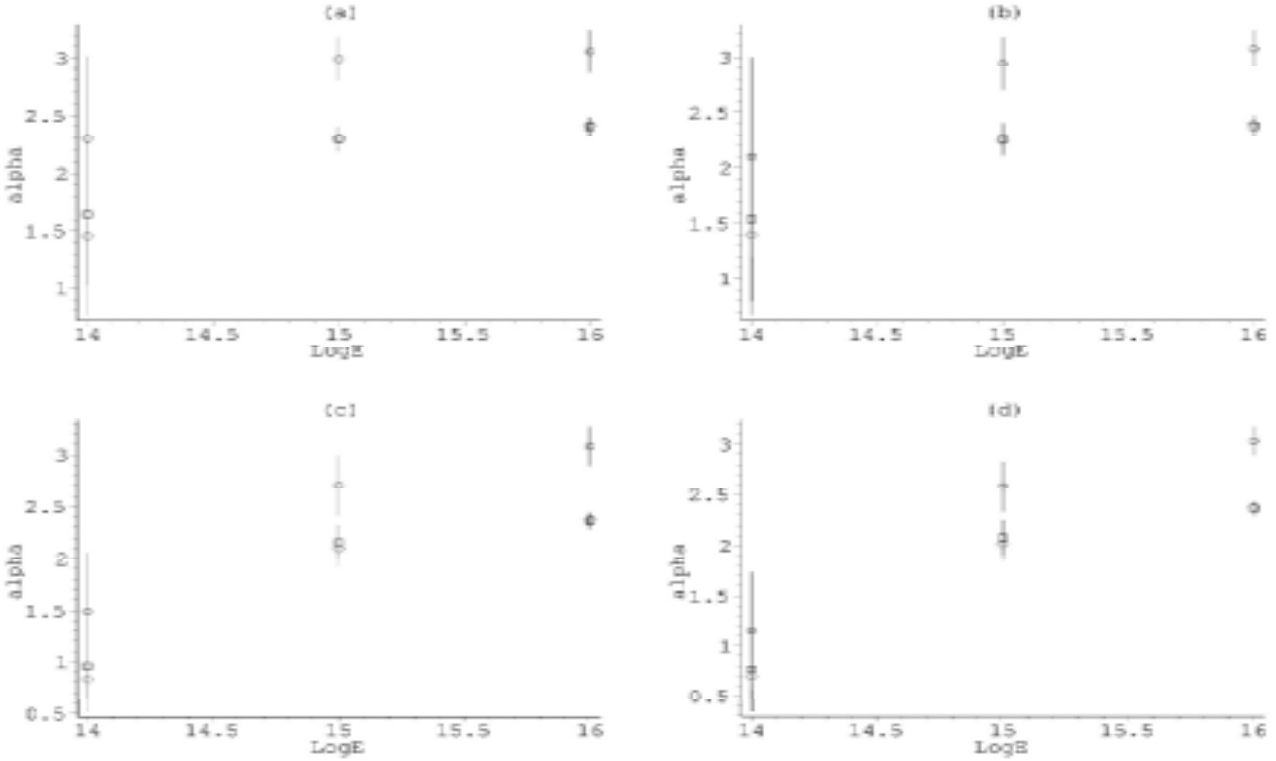

Figure 2. Fractal dimension (α) vs. shower energy for different primary types: (a) for photon, (b) for proton, (c) for Aluminum, and (d) for Iron induced showers. Circles, Boxes, and diamonds represent the data in annuli defined by $0 \le r \le 3m$, $4m < r \le 6m$, and $8m < r \le 10m$ respectively.

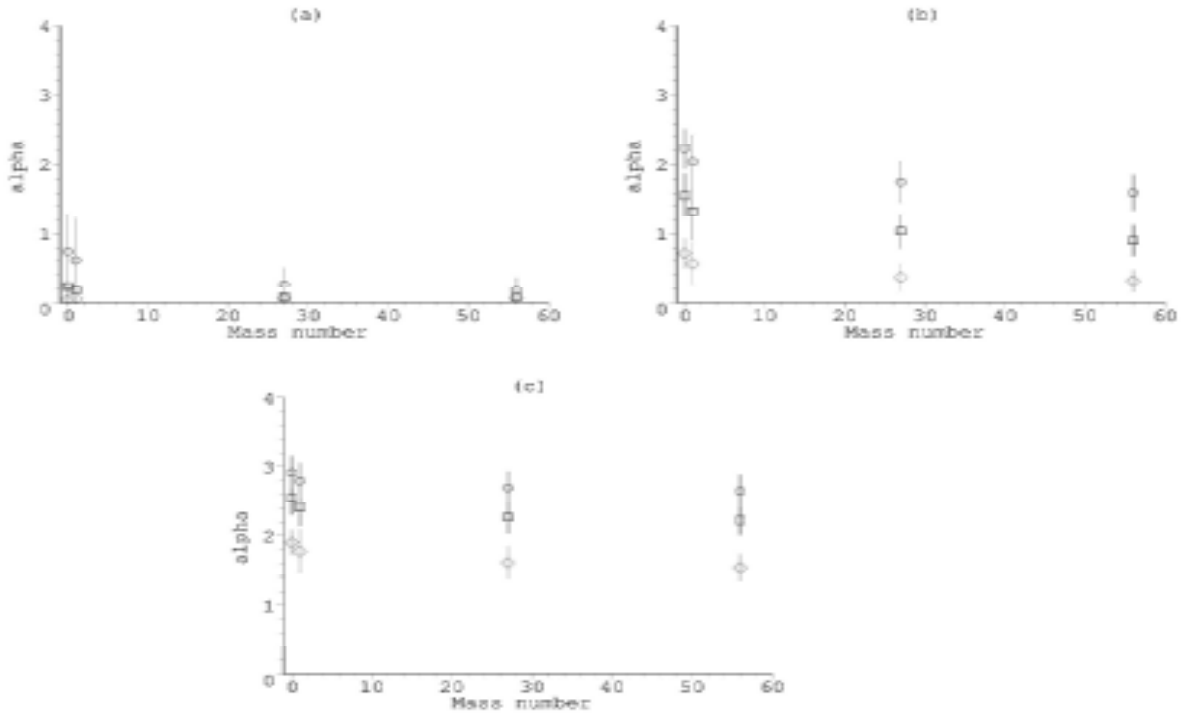

Figure 3 Fractal dimension (α) vs. mass number of primary particle for three energies at more distant areas to the core: (a) for 10^{14}eV, (b) for10^{15}eV, and (c) for 10^{16}eV showers. Circles, Boxes, and diamonds represent the data in annuli defined by $20\text{m} \le r \le 30\text{m}$, $50\text{m} < r \le 60\text{m}$, and $100\text{m} < r \le 110\text{m}$ respectively.

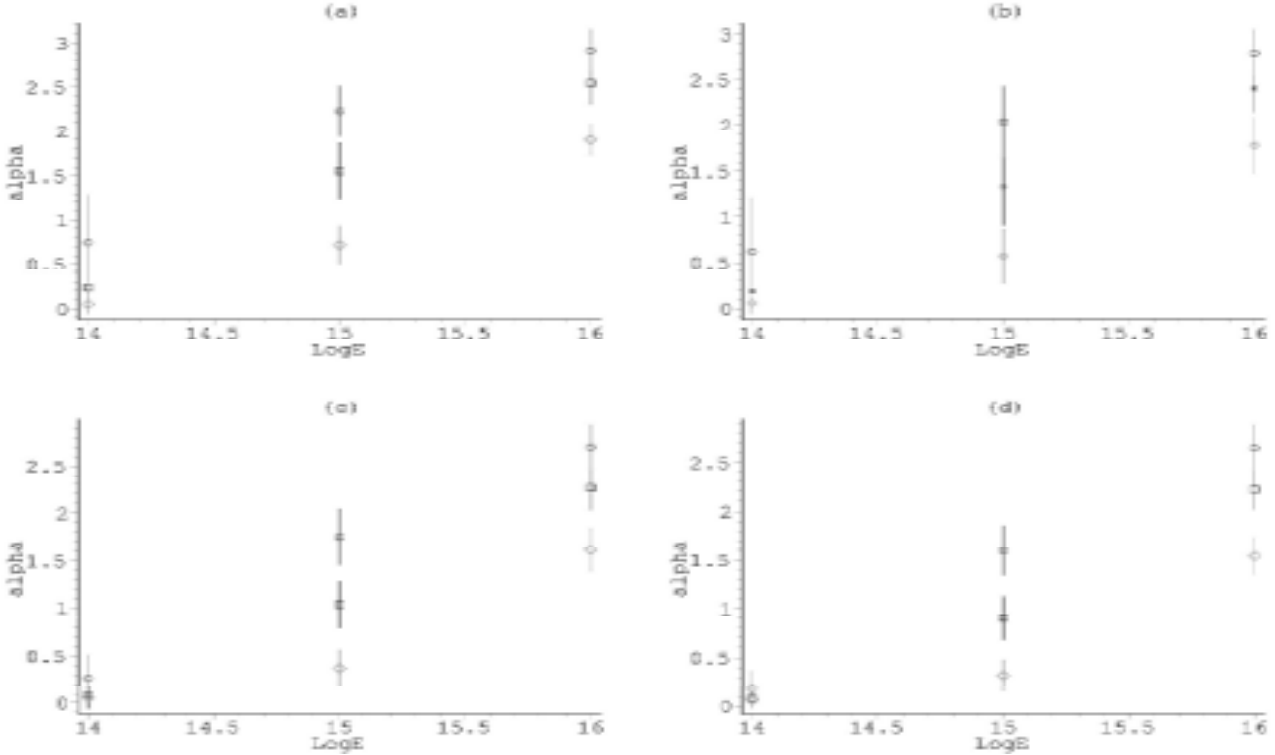

Figure 4. Fractal dimension (α) vs. shower energy for different primary types: (a) for photon, (b) for proton, (c) for Aluminum, and (d) for Iron induced showers. Circles, Boxes, and diamonds represent the data in annuli defined by $20\text{m} \le r \le 30\text{m}$, $50\text{m} < r \le 60\text{m}$, and $100\text{m} < r \le 110\text{m}$ respectively.

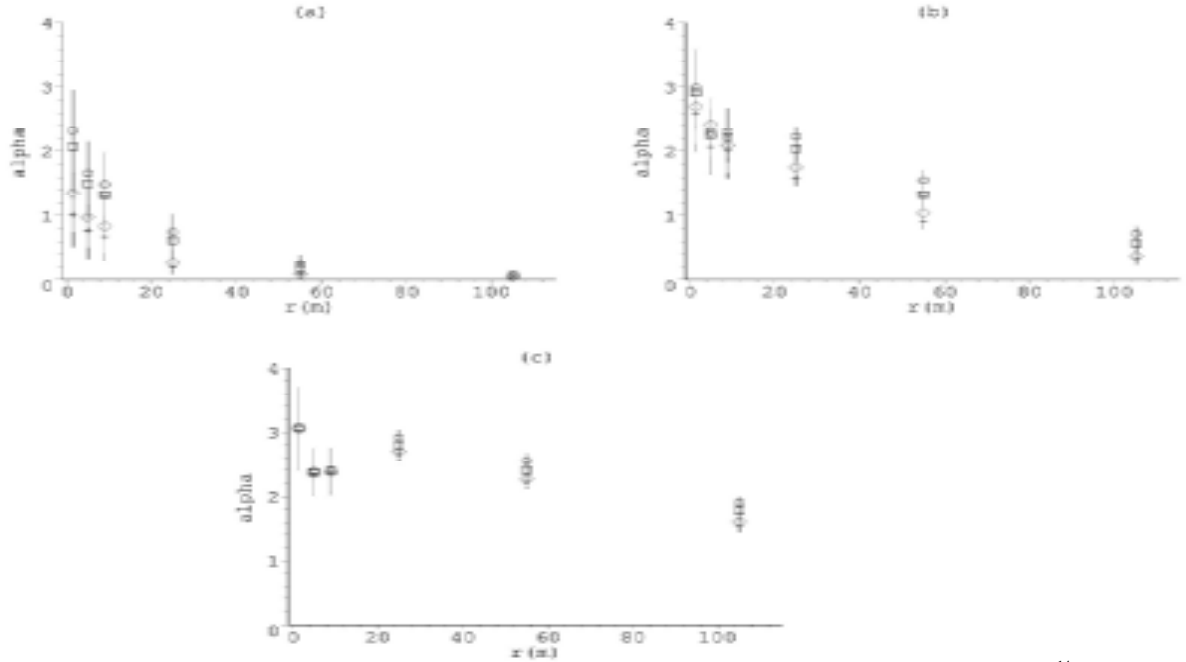

Figure 5. Fractal dimension (α) vs. core distance for showers with different primary type and energies: (a) for 10^{14}eV, (b) for 10^{15}eV, and (c) for 10^{16}eV showers. Circles, Boxes, diamonds, and crosses represent the data for showers initiated by gamma-ray, proton, aluminum, and iron respectively.

mass numbers and energies. For each fixed energy and mass number, a pair of constants p_1 and p_2 has been obtained by fitting the corresponding subset of the data to the M_{est} function. Then for each fix energy, the obtained p_1 and p_2 were fitted to a linear function of mass number separately. Table 1 summarizes the results.

Since the fit results turned to be mass dependent variables themselves, we need to take another step to get the best mass estimation. We consider $\Delta m = | M_{est} - m |$ as a function of m, the mass number, to be minimized numerically. The estimated mass number is the value which minimizes the Δm. In order to check the method for our data in different energies, half of the simulated showers in each energy were used for obtaining the energy dependent M_{est} function. Then, the mass estimation method was applied to the rest of the simulated showers. In figure 6 the histograms of the estimated mass numbers for showers with known primary particle type and energy are shown. As we have seen in the previous section, the average fractal dimension of a shower at a certain distance from the core has a normal distribution itself. In figure 1 for example, each point represents the ensamble average, and the error bars are standard deviation of these distributions. Because of such distributions in μ values, we may expect overlapping M_{est} for different primaries, as is seen for 10^{14}eV gamma and proton induced showers. Such overlaps have been reported in the previous work [20]. Despite the overlap, 77% of gamma induced showers of 10^{14}eV have $M_{est} < 0.9$, while 86% of proton induced showers of the same energy have $M_{est} > 0.9$. There is no overlap for higher energy showers. This can be due to the decrease of error bars, which are our σ_I and σ_O in the estimation function. The results show that the method gives a more precise estimation at higher energies.

4. Conclusion

In this work the wavelet-based fractal dimension analysis on secondary $e^{\pm}$ surface distribution is applied to simulated extensive air showers in different energies. The fractal dimension at a certain core distance for an ensemble of showers of the same type and energy has a normal distribution, with an average and standard deviation which depends on the type and energy of shower. The higher the energy of the shower, the lower is the difference of fractal dimension for different primary types. We think that for higher energy showers, the electron density is so high that the fractal dimension approaches its saturation value. This can also be inferred from the decrease of fluctuation (error bars) at higher energies. For higher energy showers, we found that more core distant regions still show unsaturated fractal dimensions which is primary type dependent. Although we just have computed the fractal dimension for six core distances, the results provide enough evidence for its core distance dependent in all showers. More results are needed to establish a well defined dependence on core distance. The fractal dimension also increases with

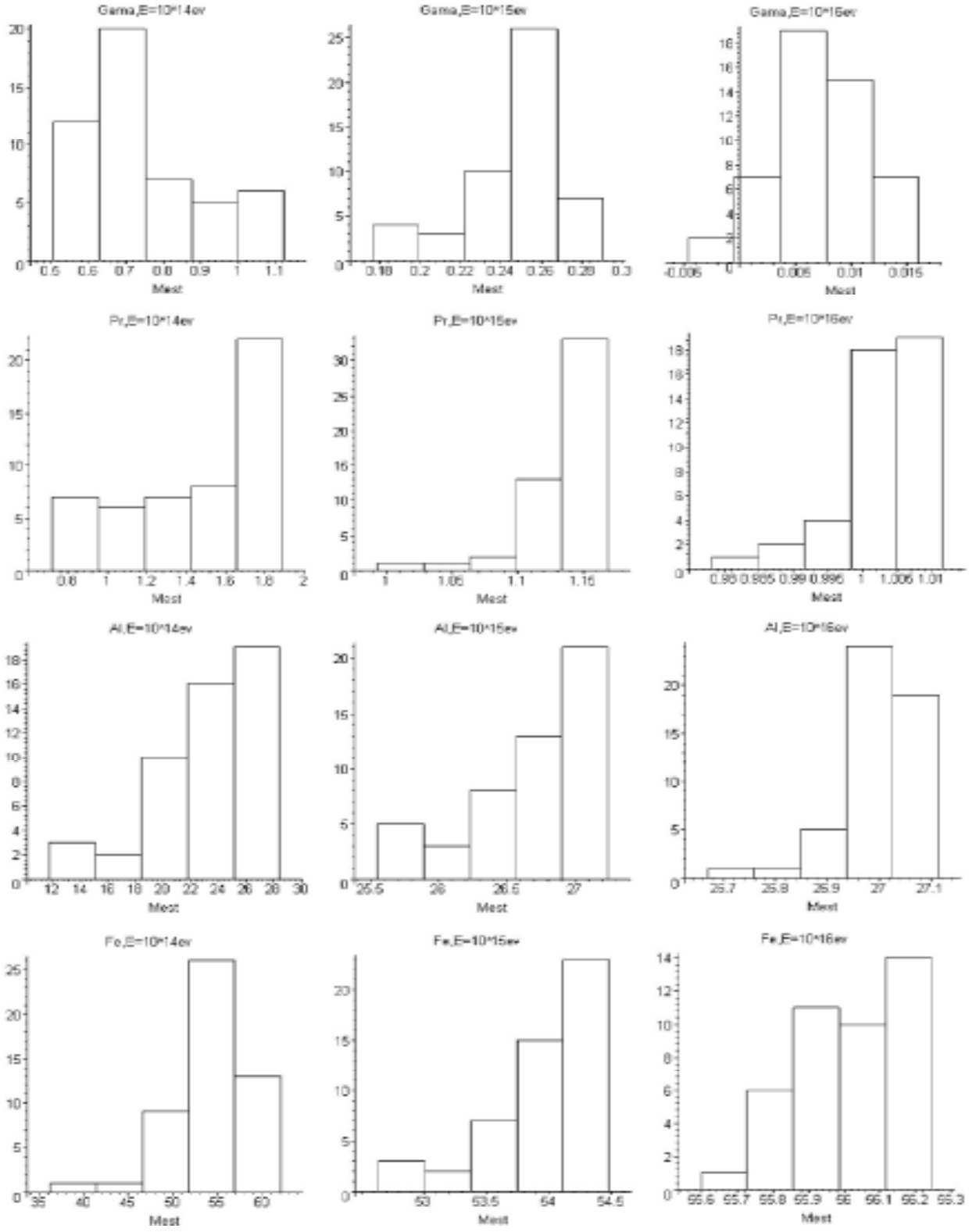

Figure 6. Histogram of estimated mass for simulated showers with different primary energy and types.

Table1. Mass number dependent parameters for M_{est} function.

shower energy	$p_1(m)$	$p_2(m)$
10^{14}eV	1.20m+3.10	-3.30m+2.13
10^{15}eV	9.34m+6.84	-21.54m-34.46
10^{16}eV	13.82m+1.23	-47.55m-8.42

shower energy at any fix distance from the core. The difference of fractal dimensions between showers of different primary types at a fix core distance decrease with shower energy. As the error bars in figures figure 1 and figure 3 show, dispersion in the fractal dimensions also decrease with energy at all core distances. Although the obtained fractal dimensions in 10^{14}eV showers, and distant regions in 10^{15}eV and 10^{16}eV showers, monotonically decrease with core distance, that is not the case for the $0 \le r \le 30m$ region around the core of 10^{15}eV and 10^{16}eV showers. Despite the energy dependent features observed in this work, the separation technique proposed by Rastegarzadeh and Samimi [20] is still applicable with relatively accurate results (see figure 6). Since the mass estimation function is tailored for each energy separately, the shower energy should be estimated independently. That means the technique is not applicable for shower energy estimation if the primary type is not known.

We should note that the separation technique discussed here are applicable for experiments with core detector in a scale of 10m capable of particle position detection. The core detector of Tibet array, equipped with emulsion chamber [29], and MWPC detectors of KASKADE [30], are suitable for this purpose. Although we have used limited computing facilities available in the present work, the open question of the mass spectrum around the knee [31,32] motivates us to extend the analysis to 10^{17-18} eV , and apply the technique to more shower type in the future.

References

1. M Bahmanabadi et al., *Exp. Astron*. **13** (2002) 1 39 .
2. J Abraham et al., (Auger Collaboration), *Nucl. Instr. Meth.* A **523** (2004) 50.
3. J A Hinton, *New Astron. Rev*. **48** (2004) 331.
4. J Belido for the Pierre Auger Collaboration, *Proc*. 29th ICRC **7** (2005) 13.
5. T Huege for LOPES Collaboration, *Nucl. Phys. Proc. Suppl*. **165** (2007) 341.
6. L O C Drury, *Rep. Prog. Phys*. **46** (1983) 973.
7. P O Lagage and C J Cesarskey, *Astron. and Astrophys*. **118** (1983) 223.
8. J K Jokipii and G Morfill, *Astrophys. J*. **312** (1987) 170.
9. W I Axford, *Astrophys. J. Suppl*. **90** (1994) 937.
10. C Fichtel and J Linsley, *Astrophys. J*. **300** (1986) 474.
11. R J Protheroe and A P Szabo, *Phys. Rev. Lett.* **69** (1992) 2885.
12. M A K Galsmacher et al., *Astropart. Phys*. **10** (1999) 291.
13. M Agrietta et al., *Astropart. Phys*. **9** (1998) 185.
14. S M Kasahara et al., *Proc. 25th Int. Cosmic Ray Conf*., Durban **4** (1997) 77.
15. M Catanese et al., *Astrophys. J*. **469** (1996) 572.
16. A Haungs and J Kempa, *Nucl. Phys*. B, *Proc. Suppl*. A **75** (1999) 248.
17. T Antoni et al., *J. Phys*. G: *Nucl. Part. Phys*. **25** (1999) 2161.
18. O V Zhurenkov and A V Plyasheshnikov, *Nucl. Phys*. B, *Proc. Suppl*. A **75** (1999) 296.
19. S P Swordy and D B Kieda, *Astropart. Phys*. **13 (**2000**)** 137.
20. G Rastegarzadeh and J Samimi, *J. Phys*. G: *Nucl. Part. Phys*. **27** (2001) 2065.
21. J Kempa, *J. Phys*. G: *Nucl. Part. Phys*. **20** (1994) 215.
22. A Haungs et al., *Nucl. Instrum. Methods* **372** (1996) 515.
23. J Kempa and M Samorski, *J. Phys*. G: *Nucl. Part. Phys*. **24** (1998) 1039.
24. C B Chiu and R C Hwa, *Phys. Rev*. D **43** (1991) 100.
25. R C Hwa and J Pan, *Phys. Rev*. D **45** (1992) 1476.
26. M Holschneidr, *J. Stat. Phys*. **50** (1988) 963.
27. A Arneodo et al., *Phys. Rev. Lett*. **61** (1988) 2281.
28. D Heck et al., *CORSIKA* (*Cosmic Ray Simulation for KASCADE*) FZKA6019 (1998) (Forschungszentrum Karlsruhe).
29. T Yuda, *Proc. Int. Symp. on Extremely High Energy Cosmic rays: Astrophysics and Future Observations*, (1996) ed. Nagano N (Inst. Cosmic Ray Res., Univ. Tokyo) 175.
30. T Antoni et al., *Astropart Phys*. **14** (2001) 245.
31. J W Fowler et al., *Astropart. Phys*. **15** (2001) 49.
32. K Bernlohr et al., *Astropart. Phys*. **8** (1998) 253.